Engineering Structures 160 (2018) 281–292

Contents lists available at ScienceDirect

Engineering Structures

journal homepage: www.elsevier.com/locate/engstruct

Experimental study on seismic behavior of steel plate reinforced concrete composite shear wall

Wei Wang[a,b], Yan Wang[a], Zheng Lu[a,c,*]

[a] Research Institute of Structural Engineering and Disaster Reduction, Tongji University, Shanghai 200092, China
[b] School of Civil Engineering, Xi'an University of Architecture and Technology, Shaanxi 710055, China
[c] State Key Laboratory of Disaster Reduction in Civil Engineering, Tongji University, Shanghai 200092, China

ARTICLE INFO

Keywords:
Steel plate reinforced concrete composite shear wall
Composite shear wall
Cyclic loading tests
Seismic behavior
Hysteretic model

ABSTRACT

Steel plate reinforced concrete composite shear wall (abbreviated as SPRW) is a novel type of composite shear wall which consists of a steel plate incased in the middle of a reinforced concrete shear wall. This arrangement aims at improving the performance of the wall, as steel plate can effectively increase the seismic behavior and concrete can protect steel plate from bulking and corrosion. In this paper, a total of 16 SPRW specimens and 3 traditional reinforced concrete (RC) walls are designed for the cyclic loading test to study the seismic performances, including failure phenomena, failure mechanism, load carrying capacity, ductility and energy dissipation characteristics, etc. Based on the extensive experimental results, the influences on the seismic behavior of SPRW are analyzed through varying parameters, e.g. aspect ratio, thickness of the wall and the steel plate, structural detailing. Finally, the hysteretic curve model and shearing capacity are generalized based on massive test data, and the design formula of shearing capacity is also proposed based on current design codes.

1. Introduction

Earthquake is an unexpected natural disaster threatening human's lives and properties. Many seismic measures have been proposed to reduce its destructive results. One way is to install dampers in the specific part of structure for controlling the dynamic response [1–6]. Another way is to optimize the current structural members to dissipate energy through the structure itself. The traditional reinforced concrete (RC) shear wall tends to develop tension cracks in the tension zones and crush in the localized compression areas during large cyclic excursions. Such cracks and crushing failures result in splitting and spalling failure of the wall with serious deterioration of stiffness and reduction in strength. Therefore, it is necessary to optimize the traditional RC shear wall for better seismic performances. On the other hand, examples of very good behavior of traditional RC wall (when properly designed) under severe input ground motions are available in literature. A couple of examples are reported in [7,8]. With the development of urbanization, the need of high-rises leads to some other directions of optimization.

Experimental results and numerical analysis indicate that the composition of steel and concrete has theoretical value and practical significance in bearing shear force [9–13], hence the composite shear wall with steel plate and concrete is proposed. To be classified by the position of the steel plate, the composite shear wall has two categories, as shown in Fig. 1. Fig. 1(a) and (b) shows composite walls whose steel plates are outside the concrete panel unilateral or bilateral. Researchers have carried out experiments on these kinds of walls and found that reinforced concrete shear walls with steel plate unilateral or bilateral both have excellent strength and ductility [14–19]. However, they have drawbacks of easier buckling of steel plates, the construction difficulty of connection between wall and floor and the erosion of steel plates.

To meet the needs of high-rise structures, steel plates can also be encased in the concrete, as shown in Fig. 1(c) and (d). The composite shear wall in Fig. 1(c) is a kind of precast shear wall. The steel frame and the steel plate are installed at the beginning, while the concrete panels are installed by bolts at the last phase of the construction [20]. In this kind of structure, the concrete panels are used only as the out-of-plane restraint, hence their material properties are not fully used. Moreover, their bolts and steel exposed in the air are easily destroyed because of fire or erosion.

The composite shear wall shown in Fig. 1(d) is a kind of cast-in-place shear wall whose reinforcements, steel channels and steel plate are arranged in order before casting. This kind of composite shear wall is the research object in this paper, which named as steel plate reinforced concrete composite shear wall (SPRW). Such structural component makes full use of steel plates and concrete and it has low

* Corresponding author at: Research Institute of Structural Engineering and Disaster Reduction, Tongji University, Shanghai 200092, China.
E-mail addresses: wangwgh@xauat.edu.cn (W. Wang), 1350756@tongji.edu.cn (Y. Wang), luzheng111@tongji.edu.cn (Z. Lu).

https://doi.org/10.1016/j.engstruct.2018.01.050
Received 1 September 2017; Received in revised form 14 January 2018; Accepted 17 January 2018

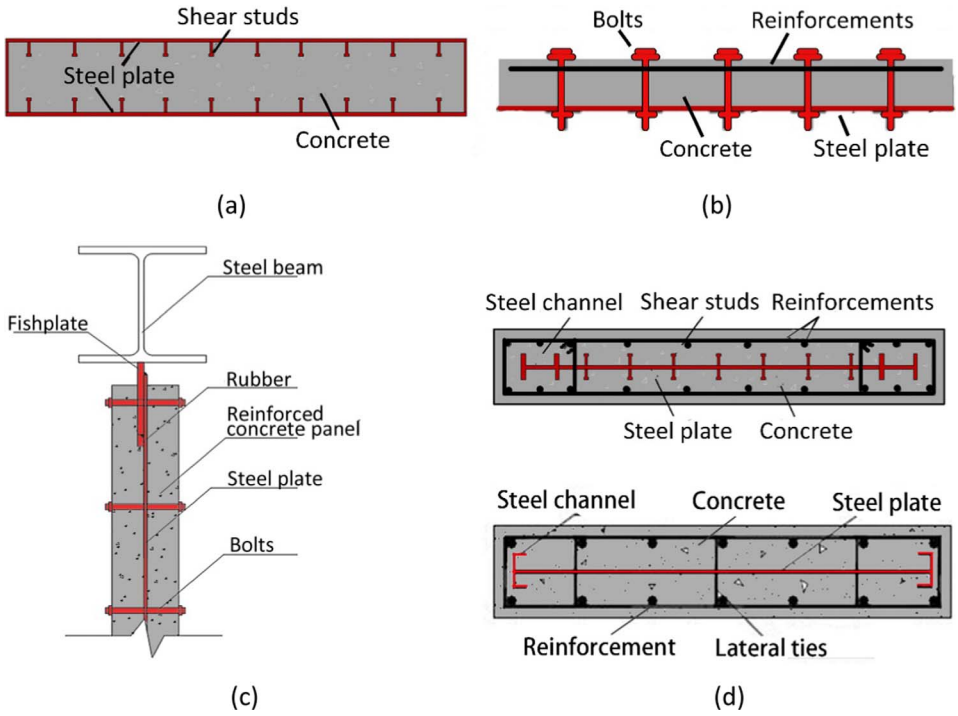

Fig. 1. Schematic diagram for steel-concrete composite shear wall. (a) Double skin steel-concrete composite wall; (b) Single skin steel-concrete composite wall; (c) Infill-plate concrete shear wall; (d) Steel plate reinforced concrete shear wall (SPRW).

requirements of fire resistance and durability.

However, there is limited understanding of such structural member no matter in practical engineering field or in theoretical research field. Wang et al. [21] simulated the steel plate reinforced concrete walls whose primary parameters varied in the axial load ratio, the ratio of steel plate and the ratio of web reinforcement in RC shear wall. However, the influence of some key parameters, such as thickness of the steel plate, thickness of the wall, aspect ratio and detailing between concrete and steel plate, on the seismic behavior of SPRWs is still short of systematic research, especially for the corresponding experimental study, which will certainly restrain the application of such structural member.

Consequently, a total of 16 SPRW specimens and 3 traditional RC walls with various parameters are tested. Their seismic performances, including failure phenomena, failure mechanism, load carrying capacity, ductility and energy dissipation characteristics are investigated. The key influence of some important parameters is also analyzed for the understanding of the seismic mechanism. Finally, the design formula of shearing capacity is also proposed based on current design codes. This paper systematically investigates the seismic behavior of SPRW, from extensive experiments, parametric study and practical design formula, which will provide reference for engineering design and promote its applications in future building constructions.

2. Experimental design

2.1. Specimen design

A total of 16 SPRW specimens are designed at the scale of 1:2. The properties are listed in Table 1, and the details are shown in Fig. 2. Another three parallel specimens of traditional RC walls equivalent in dimensions are also designed as a control group. To study the seismic behaviors of SPRWs, a cyclic quasi-static test is carried out at the State Key Laboratory of Disaster Reduction in Civil Engineering, Tongji University. The test setup consists of vertical and horizontal loading devices. Axial load is applied by four ball-bearing hydraulic jacks whose oil pump is manually controlled to ensure that the axial load remains constant. Lateral cyclic load is applied by the horizontal actuator with one end fixed on the reaction wall and the other on the loading beam. The test setup is shown in Fig. 3.

Seven linear variable displacement transducers (LVDTs) are horizontally placed on the model at the level of mid-height, top and bottom of the specimen. LVDT at the top level aims at measuring top movement of the SPRW for drawing its hysteretic curve, while LVDT at the bottom level is used to monitor whether the specimen slide during the test. Another four LVDTs are fixed on two sides and the diagonal directions of the specimen to observe whether the wall distorts.

The force and displacement-controlled loading history is adopted in this test. Before the specimen yields, force-controlled multi-stage loading is applied. The initial load is 25% of the estimated yield load, and it has an increase of 10 kN or 20 kN per level (according to the aspect ratio of the specimen). The difference between the levels should be reduced when it is close to the estimated cracking or yield load. For each level, one cycle is performed. After the specimen yields, displacement-controlled multi-stage loading is applied, whose level difference is 2 mm. For each displacement level, three cycles are performed. The horizontal forces are applied under controlled cyclic displacements until the strength of the specimens decreases to 85% of the peak horizontal load. The method to determine yield point of the specimen is the same as introduced in literatures [14,16], which is mainly evaluated by its definition. When the hysteretic curve abruptly changes, the specimen is considered to be yielded. The loading history is illustrated in Fig. 4.

2.2. Material properties

In the specimens, the steel plates are made of Grade Q235 steel. Tension tests have been performed on steel plates and steel bars, whose results are shown in Table 2. There are two kinds of concrete, C30 and C50. The test cubes and the specimens are fabricated, casted and cured simultaneously. The size of the test cube is 150 mm × 150 mm × 150 mm. The cube compressive strength test is performed on test cubes after 28 days' natural maintenance and on the same day of the test respectively. The results can be seen in Table 3.

Table 1
Properties of test specimens.

No.	Width × thickness (mm × mm)	Aspect ratio	Concrete grade	Steel plate thickness (mm)	Steel ratio (%)	Steel channel	Axial force ratio	Detailing between steel plate and concrete
SPRW1	1000 × 125	2.0	C30	4	4.23	[6.3 (63 × 40 × 4.8)	0.5	None
SPRW2	1000 × 125	2.0	C30	6	5.67	[6.3 (63 × 40 × 4.8)	0.4	None
SPRW3	1000 × 125	2.0	C50	4	4.23	[6.3 (63 × 40 × 4.8)	0.3	Lateral ties
SPRW4	1000 × 125	2.0	C50	4	4.23	[6.3 (63 × 40 × 4.8)	0.3	Shear studs
SPRW5	1000 × 125	2.0	C50	4	4.23	[6.3 (63 × 40 × 4.8)	0.3	Both
SPRW6	1000 × 200	2.0	C30	6	3.72	[8 (80 × 43 × 5.0)	0.4	None
SPRW7	1000 × 200	2.0	C30	4	2.82	[8 (80 × 43 × 5.0)	0.4	Lateral ties
SPRW8	1000 × 200	2.0	C50	4	2.82	[8 (80 × 43 × 5.0)	0.3	Shear studs
SPRW9	1000 × 125	1.5	C30	4	4.23	[6.3 (63 × 40 × 4.8)	0.4	None
SPRW10	1000 × 125	1.5	C30	6	5.67	[6.3 (63 × 40 × 4.8)	0.4	None
SPRW11	1000 × 125	1.5	C50	4	4.23	[6.3 (63 × 40 × 4.8)	0.3	Lateral ties
SPRW12	1000 × 125	1.5	C50	4	4.23	[8 (80 × 43 × 5.0)	0.3	Shear studs
SPRW13	1000 × 125	1.5	C50	4	4.23	[6.3 (63 × 40 × 4.8)	0.3	Both
SPRW14	1000 × 200	1.5	C30	6	3.72	[8 (80 × 43 × 5.0)	0.4	None
SPRW15	1000 × 200	1.5	C30	4	2.82	[8 (80 × 43 × 5.0)	0.4	Lateral ties
SPRW16	1000 × 200	1.5	C50	4	2.82	[8 (80 × 43 × 5.0)	0.3	Shear studs
RCW1	1000 × 125	2.0	C30	None	0	None	0.5	Lateral ties
RCW2	1000 × 125	2.0	C30	None	0	None	0.4	Lateral ties
RCW3	1000 × 200	2.0	C50	None	0	None	0.3	Lateral ties

Notes: Here “both” means both lateral ties and shear studs are used. RCW1 ~ RCW3 are in the control group, which are used to be compared with SPRW specimens. ∅6@300 lateral ties are spot welded with steel fabric in plum blossom form through the holes on the steel plate. 25 mm ∅6@300 studs are welded on steel plate in plum blossom form. The reinforcement of RC web panel consists of ∅6@150 vertical bars and ∅6@150 horizontal bars.

3. Experimental phenomena

3.1. Failure characteristic and mechanism

The failure characteristic of 16 SPRWs and 3 RCWs are variable; however, the failure mode of SPRWs can be roughly divided into 3 types, namely “bending mode failure”, “bending and shear failure” and “foundation anchor failure” according to the aspect ratio and thickness of the wall (Fig. 5). In general, specimens with larger aspect ratio and thinner wall tend to damage in “bending mode failure”, while specimens with smaller aspect ratio and thicker wall tend to damage in “bending and shear failure”. As the capacity and stiffness of “short and thick wall” are relatively better in all the specimens, the strength of the foundation anchorage is relatively smaller than that of the wall. Hence some “short and thick” specimens are damaged at the foundation.

Due to different concrete strength and detailing, “bending mode failure” can be divided into “initiated by shear slip failure” and “initiated by shear compression failure”. The two sub-categories explain the reason why the specimen begins to damage. When the strength of concrete is low, concrete and steel plate at middle-lower part tend to slip, finally leading to buckling and failure (“initiated by shear slip failure”). When the concrete is high in strength with studs, the wall shows ductility and finally, the concrete at the corner crushes (“initiated by shear compression failure”). From the view of the whole specimen’s failure mode, specimens are characterized as “bending mode failure” whose steel plate or reinforcement is yielded before failure.

For all the SPRW specimens, the earliest crack appears at the middle-lower part. Specimens with detailing between steel plate and concrete have higher cracking load. With the shear force growing, the cracks develop to middle-higher part and gradually form transverse cracks with concrete at the corner crushes. Specimens with different failure modes have their specific characteristics.

For specimens of “initiated by shear slip failure” as shown in Fig. 6(a), concrete at the corner crushes and spalls along the direction of the cracks before shear force reaches the ultimate load. As bonding effect between concrete and steel plate is relatively poor, reinforcements at edge of the bottom buckle or even fracture. The cover of the concrete crushes and gradually develops into broken zones that are as

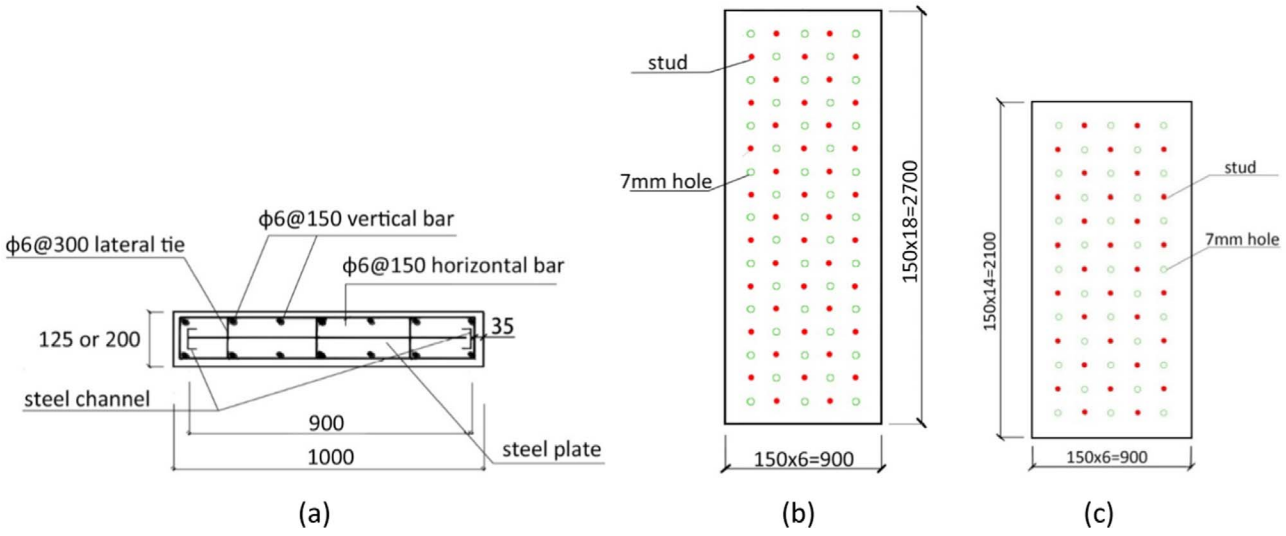

Fig. 2. Details of the specimens. (a) Cross section of SPRW; (b) and (c) Details of the steel plates (Units in mm).

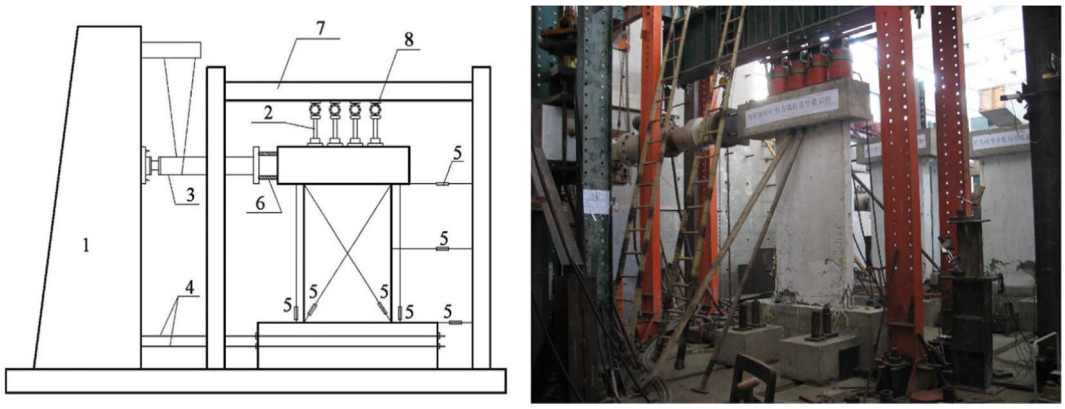

Fig. 3. Test setup. (a) Schematic diagram, 1 – reaction wall, 2 – hydraulic jacks, 3 – hydraulic actuator, 4 – base anchor, 5 – LVDT, 6 – anchor rod, 7 – loading frame, 8 – ball bearing; (b) Test photo.

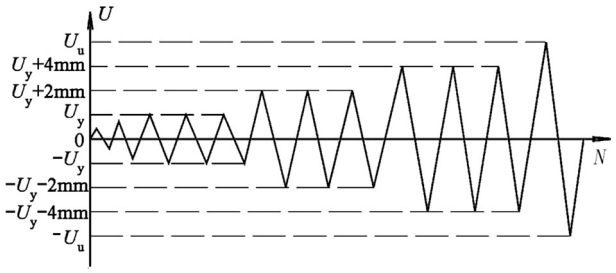

Fig. 4. Diagram for load history.

Table 2
Properties of steel plates and steel bars (MPa).

	No	Elastic Modulus/10^5	Yield Strength	Ultimate tensile strength
4 mm steel plate	1–1	1.86	297.3	410.3
	1–2	1.86	304.1	419.1
	1–3	1.99	304.9	412.4
	Mean value	1.90	302.1	413.9
	Standard deviation	0.08	4.2	4.6
6 mm steel plate	2–1	1.98	283.1	403.1
	2–2	2.03	352.9	480.3
	2–3	2.02	302.0	450.1
	Mean value	2.01	312.7	444.5
	Standard deviation	0.03	36.1	38.9
Φ6 steel bar	3–1	1.98	324.6	377.6
	3–2	1.97	383.8	438.1
	3–3	2.02	334.9	412.6
	Mean value	1.99	347.76	409.45
	Standard deviation	0.03	31.61	30.39

thick as the thickness of the wall, and finally leads to out-of-plane instability of the specimen. At the same time, steel plate and steel channel at the bottom buckles severely, as shown in Fig. 7 (SPRW7 and SPRW9).

For specimens of “initiated by shear compression failure” as shown in Fig. 6(b), the concrete at the corner slightly crushes when the cracks at middle-higher part no longer develop and stay relatively steady. At that time, shear force reaches its maximum. With the lateral displacement increasing, damage at the corner develops slowly. At last, the bearing capacity decreases to 85% of the maximum capacity as concrete at the corner crushes and spalls, and reinforcements fracture. The specimens show ductility during the loading process. The steel plates

Table 3
Properties of concrete (MPa).

Concrete mark	No	28 days		The day of the test	
		f_{cu}	f_c	f_{cu}	f_c
C30	1–1	32.00	15.29	31.76	18.23
	1–2	29.38	14.03	35.57	14.79
	1–3	24.89	11.89	37.62	17.12
	Mean value	28.76	13.74	34.98	16.71
	Standard deviation	3.60	1.72	2.97	1.76
C50	2–1	49.33	23.57	51.59	24.14
	2–2	52.44	25.05	53.20	25.97
	2–3	47.11	22.51	47.87	22.83
	Mean value	49.64	23.71	50.89	24.31
	Standard deviation	2.68	1.28	2.73	1.58

Notes: f_{cu} is the measured value of concrete cube compressive strength; f_c is the design value of concrete compressive strength.

show small deformation when concrete is knocked out after the experiment.

For specimens of “bending and shear failure” as shown in Fig. 6(c), the cracks on the concrete panel become steady when the shear force reaches its maximum. Then concrete at the corner crushes and grows slowly as the lateral displacement increases. But the horizontal shear cracks at bottom of the wall become increasingly obvious. Finally, concrete at the corner spalls and the reinforcements fracture. The specimens show ductile failure and the deformation of the steel plates are not obvious, as shown in Fig. 7 (SPRW14).

For specimens of “foundation anchor failure” as shown in Fig. 6(d), the test phenomena are similar to specimens of “bending and shear failure”, and their bearing capacity, stiffness and ductility are better than other specimens. Because the foundation anchorage is relatively poorer than the wall strength, the cracks appear between bottom beam and the wall.

Traditional reinforced concrete shear walls as shown in Fig. 6(e) shows obvious “shear failure”. All the plastic crack developments concentrate at the bottom of the specimen. At later stage of the loading, the specimen suddenly destroys when its stiffness and load still remain steadily.

The failure mechanism of SPRW can be concluded according to the experiment phenomena as follows:

(1) Before cracking (about 60%F_{max}), concrete, steel plate and steel bars cooperate well with each other to carry lateral forces, in which the concrete carries more loads.
(2) After cracking, more and more concrete exits from working with the

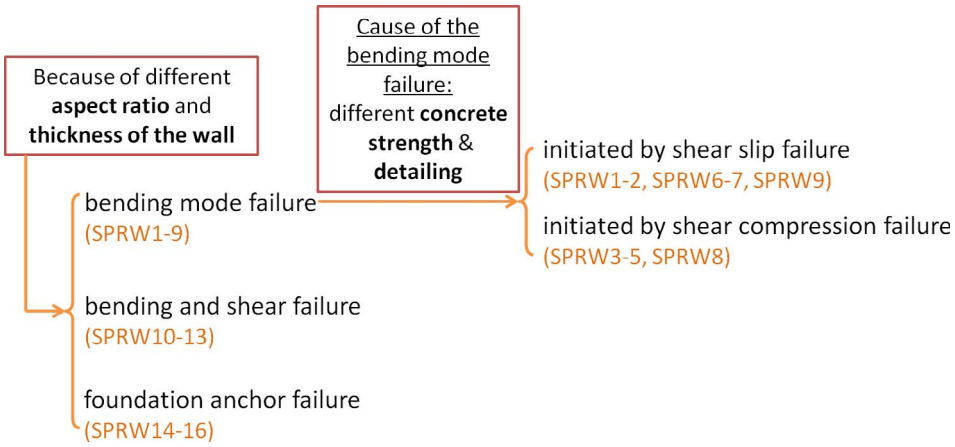

Fig. 5. Failure mode of SPRW.

development of cracks. Thus loads are distributed to steel plate and steel bars until the member yields (about 80% F_{max}).

(3) When steel bars in the margin of the wall buckle or yield as they subject to moment and shear force repeatedly, cracks of the concrete extend steadily, and the lateral force reaches its peak F_{max}. At this time, steel plate plays the major role in carrying lateral forces, while concrete provides lateral restraint for steel plate. Therefore, concrete prevents steel plate from premature failure in stability.

(4) The failure mode differs from each other because parameters, such as aspect ratio of the wall, thickness of the steel plate, strength of the concrete and structural detailing, are different.

3.2. Hysteresis curves and skeleton curves

Lateral force-displacement hysteresis curves are drawn according to the cyclic loading test, shown in Fig. 8. There is no special meaning for these colors, just for distinguishing different load cycles. Skeleton curves can be obtained from hysteresis curves, as shown in Fig. 9. It can be observed from Figs. 8 and 9(a) that lateral capacity and deformability of specimens with steel plates (SPRW1-8) are far better than those of the traditional shear walls (RCW1-3).

In Fig. 9(a), the lateral capacity of SPRW6, SPRW 7 and SPRW 8 is better than SPRW1-5, because they have thicker walls. SPRW1 and SPRW2 have poor deformability for lack of necessary detailing between concrete and steel plate, while SPRW3-5 perform better with lateral ties or shear studs, in which SPRW5 (with both lateral ties and shear studs) is the best. Similar conclusions can be obtained from specimens in Fig. 9(b), whose aspect ratio is different from that in Fig. 9(a).

3.3. Ductility factor and equivalent viscous damping coefficient

Ductility can reflect plastic deformability of the structural members. In this paper, ductility is evaluated by displacement ductility factor, which is defined as the displacement corresponding to the ultimate load dividing the displacement at the yield load. As can be seen in Table 4, the ductility factor of SPRW8 and SPRW13 is larger than 4.0, excelled in specimens. This is mainly because of relatively larger thickness or proper detailing.

Energy dissipating capacity of the specimen can be calculated by the area encircled by the load-displacement hysteresis curves. The index of energy dissipating capacity includes energy dissipating factor, equivalent viscous damping coefficient and working index, etc. Equivalent viscous damping coefficient h_e is selected here to evaluate specimens' energy dissipating capacity, shown in Table 4. The equivalent viscous damping coefficient (Fig. 10) is the ratio of the energy stored in the specimen to the deformation energy of the specimen in the elastic phase. The formula is as follows:

$$h_e = \frac{1}{2\pi}\frac{area\ (ABC)}{area\ (OBD)} \quad (1)$$

The thickness of the wall is the most important parameter to increase equivalent viscous damping coefficient h_e, followed by detailing and thickness of the steel plate.

It can be concluded from Table 4 that thickness of the wall and thickness of the steel plate are the main factors with regard to bearing capacity, while setting shear studs or lateral ties is important as far as ductility or energy dissipation is concerned.

4. Seismic analysis of SPRWs with different parameters

4.1. Aspect ratio

Two types of aspect ratio are adopted in the test, 1.5 and 2.0. As can be seen from the experimental phenomena, aspect ratio plays a critical role in the failure mode of the wall. SPRW1-SPRW8, whose aspect ratio is 2.0, can be classified to bending mode damage, because damage stems from the development of the main bending crack, which finally leads to yielding in the steel member on the edge of the wall and crushing in the concrete at the bottom of the wall. Damage of SPRW9 ~ SPRW16, whose aspect ratio is 1.5, is controlled by horizontal crack at the bottom of the concrete, except SPRW9. Although SPRW9 is small in aspect ratio, its failure mode is bending mode damage, which is different from other specimens with the same aspect ratio. This is because its concrete is low in strength with thin steel plate and there is no binding between concrete and steel plate, which tends to result in out-of-plane instability. In addition, specimens with the aspect ratio of 2.0 show greater energy dissipation capacity than those of 1.5 ones in light of the h_e values (Table 4), which is determined by their failure modes.

4.2. Thickness of the wall

The thickness of the wall can be classified into 125 mm and 200 mm. The thicker specimens have higher yielding and ultimate capacity according to the test result (Table 4). That is to say, the thicker the concrete cover out of the steel plate is, the larger lateral capacity the specimen has. The deformability of thicker specimens is larger from the perspective of ultimate displacement and ultimate displacement angles. This is because concrete can provide stronger lateral resistance for steel plate, and therefore, prevents the steel plate from premature failure in stability and increases deformation capacity of the wall.

4.3. Thickness of the steel plate

The deformability, stiffness, bearing capacity and energy dissipation capacity of SPRW is far better than traditional RC shear wall. A thicker

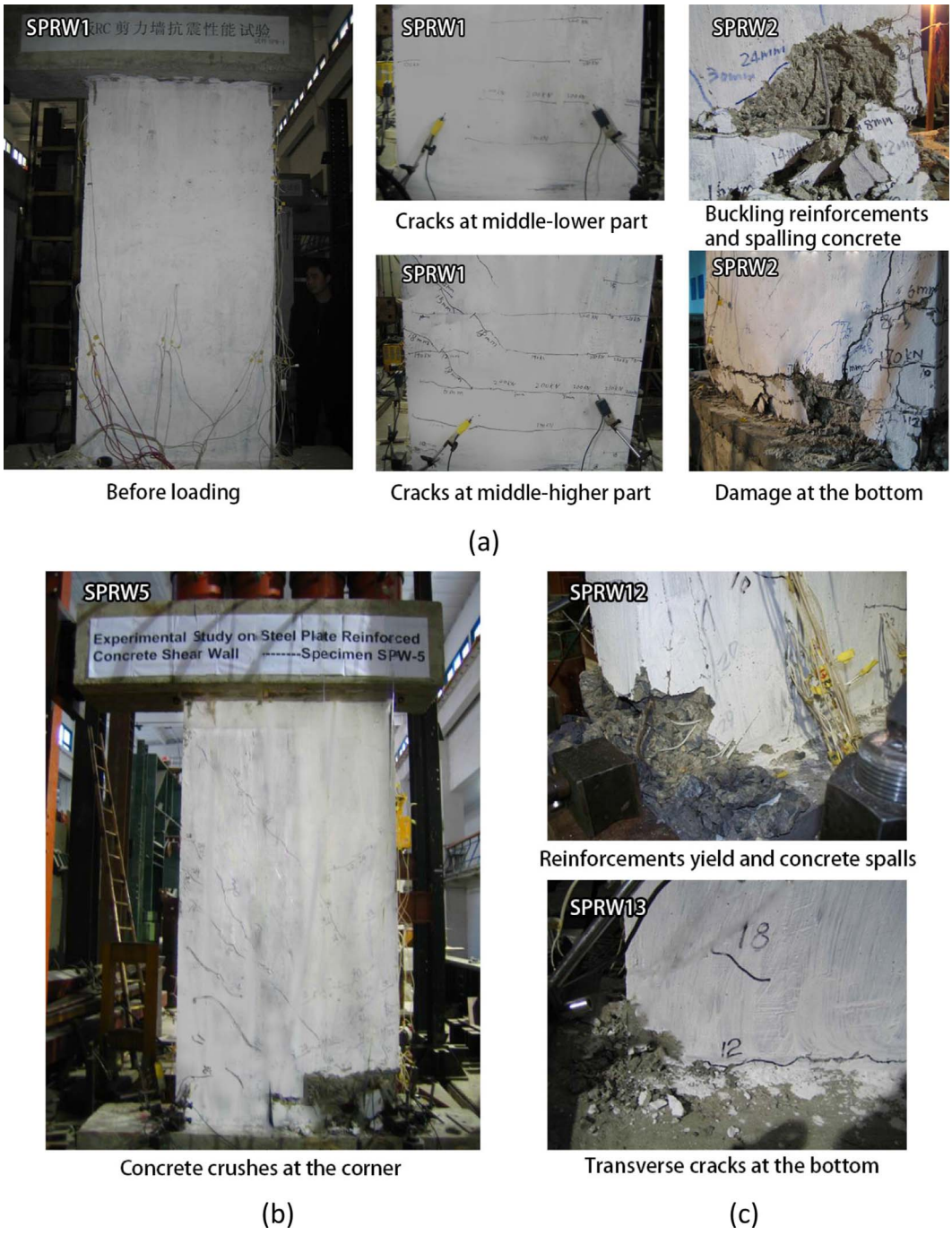

Fig. 6. Failure pattern and crack distribution. (a) Shear slip failure; (b) Shear compression failure; (c) Bending and shear failure; (d) Foundation anchor failure; (e) Shear failure.

steel plate should be better than a thinner one. Compared with specimen SPRW9 (4 mm), energy dissipation and lateral displacement of SPRW10 (6 mm) is obviously better. As for vertical and lateral bearing capacity, a thicker steel plate can distinctly increase the capacity.

4.4. Structural detailing

Some papers [22,23] about SPRWs have mentioned that the connection between steel plate and concrete is important. Therefore, two types of structural detailing, shear studs and lateral ties have been used in the test specimens. The test results indicate that specimens with shear studs develop steadily in crack extension and less in crack amount in contrast to the other ones. This is understandable since the studs have an active effect in mitigating cracking, thus combining two components together well. On the other hand, this detailing is appropriate to improve the retention of post-peak strength, which leads to ductility failure. However, lateral ties provide less improvement in strength, deformability and ductility than shear studs. They only contribute to lessening crack development barely at the early cycles of loading [24].

4.5. Axial compression ratio

Axial compression ratio is a critical index in seismic design. Generally, proper vertical load is beneficial to the bearing capacity and lateral stiffness of the shear wall. But it may lead to brittle failure if axial compression ratio is too large. In this experiment, specimen has better ductility when axial compression ratio is smaller (SPRW1 and

Crack between bottom beam and wall

Transverse crack at the bottom

Cracks concentrates at the bottom

(d) (e)

Fig. 6. (*continued*)

Fig. 7. Deformation of the steel plates.

SPRW2). In practical engineering projects, encasing steel plate into the RC shear wall can significantly increase its vertical capacity and reduce the axial compression ratio, thus increasing ductility.

4.6. Comparison between SPRWs and traditional RC walls

Comparing the index of seismic behavior of SPRW and RC shear wall, it is shown that the SPRWs exhibit ductility failure. The load capacity, ultimate displacement, the ductility index and equivalent viscous damping coefficient of SPRWs are increased by 106.99%, 121.96%, 25.02% and 24.99% on average, respectively, compared with RCW specimens. The hysteretic curve seems plumper, as can be seen in Fig. 8. Although it seems that the reinforcement ratio of the SPRW and the RCW are different, previous researches [25–27] indicate that increasing amount of conventional longitudinal and horizontal reinforcement in RC walls cannot effectively improve its seismic performance and avoid adverse damage modes. Therefore, steel plate has a significant effect on enhancing the seismic behavior of a structural member, that is, SPRW has larger shear stiffness with smaller thickness and less weight when the capacity is the same as RC shear wall, which

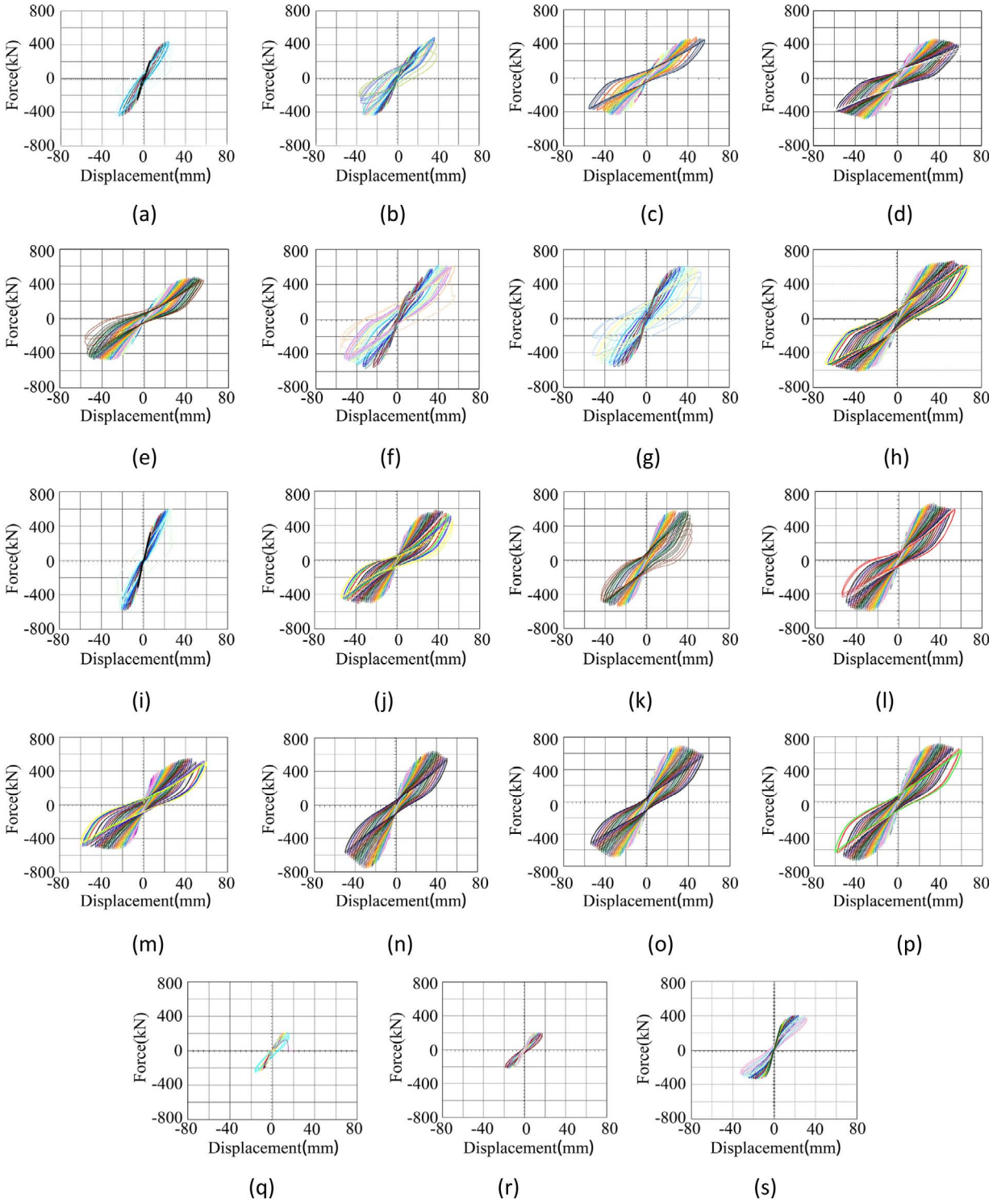

Fig. 8. Lateral force-displacement hysteresis loops. (a)-(p) SPWR1-16; (q-s) RCW1-3.

not only enhance space utilization, but also reduce the size of the foundation, and at the same time, the seismic action is reduced.

5. Generalized hysteretic curve model and shearing capacity

5.1. Hysteretic curve model generalization

5.1.1. Skeleton curve

Hysteretic curve model can be generalized based on fitting the test data, including acquiring the key point of the skeleton curve and the description of hysteretic rule. There are many factors affecting hysteresis loop of compression-flexure member, including axial compression ratio, aspect ratio, material properties etc. However, reasonable regularity relationship can still be obtained by using dimensionless coordinates, because this usually reflected the force mechanism or physical nature of such members [28,29]. Shear wall is a shear member without exact explicit yield point (unlike the flexural member). According to literatures [30–32], the definitions of yield displacement include first yield method, equivalent elasto-plastic method, equivalent elasto-plastic energy absorption method, reduced stiffness equivalent

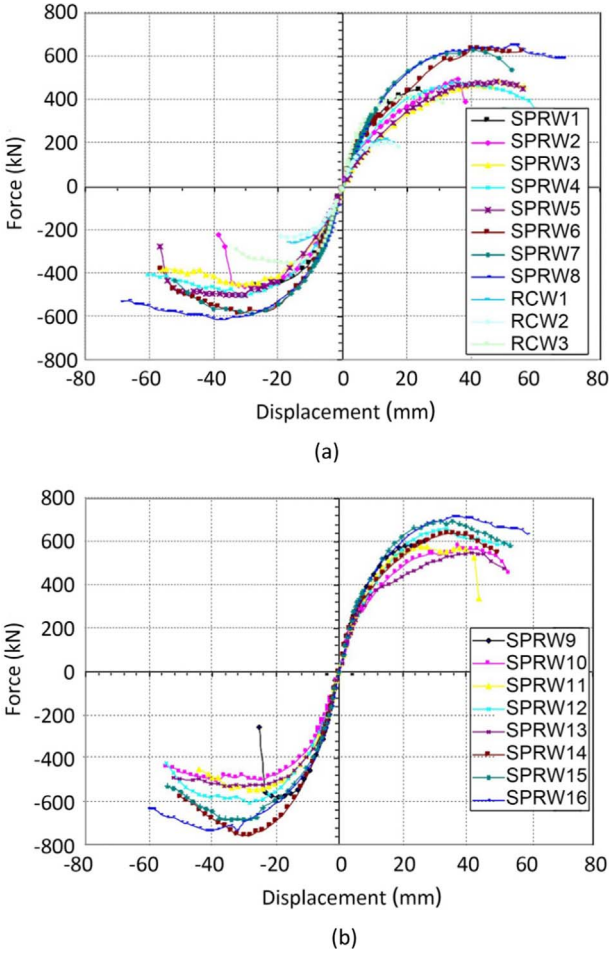

Fig. 9. Skeleton curves. (a) SPRW1-SPRW8 and RCW1-RCW3; (b) SPRW9-SPRW16.

elasto-plastic method and general yield moment method, etc. The yield points obtained by different methods have great distinctions in value, hence they are not utilized in this paper. On the other hand, the maximum load point is defined as the point of peak horizontal load during the cyclic load, which has much clear definition and relatively stable and explicit value; consequently, the maximum load point (F_{max}, Δ_{max}) is chosen as the datum point. The skeleton curves of 16 SPRWs are

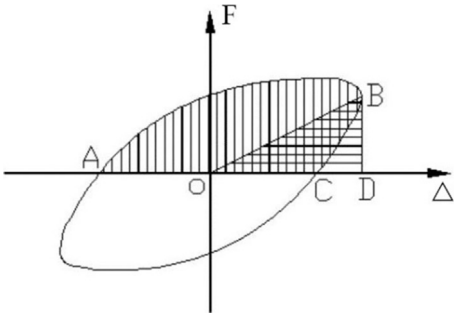

Fig. 10. The calculation diagram of equivalent viscous damping coefficient.

nondimensionalized, which can be seen in Fig. 11(a).

Through linear regression analysis of non-dimensional skeleton curves, the coordinate of cracking point A is (0.24, 0.6), which approximately agrees with the tested cracking point (i.e. the load level when initial crack can be seen by naked eyes); the coordinate of yield point B is (0.46, 0.8), which approximately agrees with the yield point defined according to the secant stiffness at $0.75F_{max}$ (Fig. 12); the coordinate of peak point C is (1.0, 1.0), and the coordinate of ultimate displacement D is the corresponding point of $0.85F_{max}$. The expression of the four-line skeleton curve can be obtained in Eq. (2), and the skeleton curve is shown in Fig. 11(b).

$$\left.\begin{array}{ll} OA\text{: } F/F_{\max} = K_1\Delta/\Delta_{\max} & (K_1 = 2.5, 0 \leqslant \Delta/\Delta_{\max} \leqslant 0.24) \\ AB\text{: } F/F_{\max} = K_2\Delta/\Delta_{\max} + 21/55 & (K_2 = 10/11, 0.24 \leqslant \Delta/\Delta_{\max} \leqslant 0.46) \\ BC\text{: } F/F_{\max} = K_3\Delta/\Delta_{\max} + 17/27 & (K_3 = 10/27, 0.46 \leqslant \Delta/\Delta_{\max} \leqslant 1) \\ CD\text{: } F/F_{\max} = K_4(\Delta/\Delta_{\max} - 1) & (K_4 < 0.1 \leqslant \Delta/\Delta_{\max} \leqslant \Delta_u/\Delta_{\max}) \end{array}\right\} \quad (2)$$

The slope of the descending stage K_4 is related to ductility coefficient μ, and its value is negative. $\Delta_u/\Delta_{max} = 0.46\mu$ can be derivated from equation $\mu = \Delta_u/\Delta_y$ and regression analysis result $\Delta_y = 0.46\Delta_{max}$. Consequently,

$$K_4 = \frac{0.15}{1 - 0.46\mu} \quad (3)$$

5.1.2. Standard hysteresis loop

The standard hysteresis loop near yield point and peak point can be obtained in the similar way of fitting skeleton curve. Tri linear is adopted to represent standard hysteresis loop. The standard hysteresis loop near yield point can be described by Eq. (4).

Table 4
Seismic performance Index of test specimens.

No.	Yield load (kN)	Peak load (kN)	Yield displacement (mm)	Ultimate displacement (mm)	Ductility factor	h_e (when destroyed)
SPRW1	365	437	8.6	19.7	2.29	12.58
SPRW2	366	450	10.8	28.3	2.62	18.00
SPRW3	369	439	17.0	42.9	2.52	14.21
SPRW4	366	471	16.9	45.4	2.68	15.60
SPRW5	370	473	16.2	46.9	2.89	15.98
SPRW6	451	585	11.8	46.3	3.94	18.11
SPRW7	464	581	10.3	39.2	3.80	20.54
SPRW8	519	601	12.8	52.4	4.08	20.84
SPRW9	484	593	6.9	17.0	2.45	9.42
SPRW10	472	537	10.3	28.8	2.81	11.98
SPRW11	460	567	8.3	30.4	3.65	11.30
SPRW12	523	625	12.1	35.1	2.90	11.64
SPRW13	418	531	7.9	38.6	4.89	11.87
SPRW14	578	698	12.5	34.1	2.72	12.59
SPRW15	557	693	11.8	34.8	2.95	12.18
SPRW16	624	727	12.8	37.8	2.95	13.20
RCW1	204	233	6.5	9.9	1.52	10.89
RCW2	179	212	5.5	13.8	2.51	11.36
RCW3	354	371	7.2	25.1	3.49	12.26

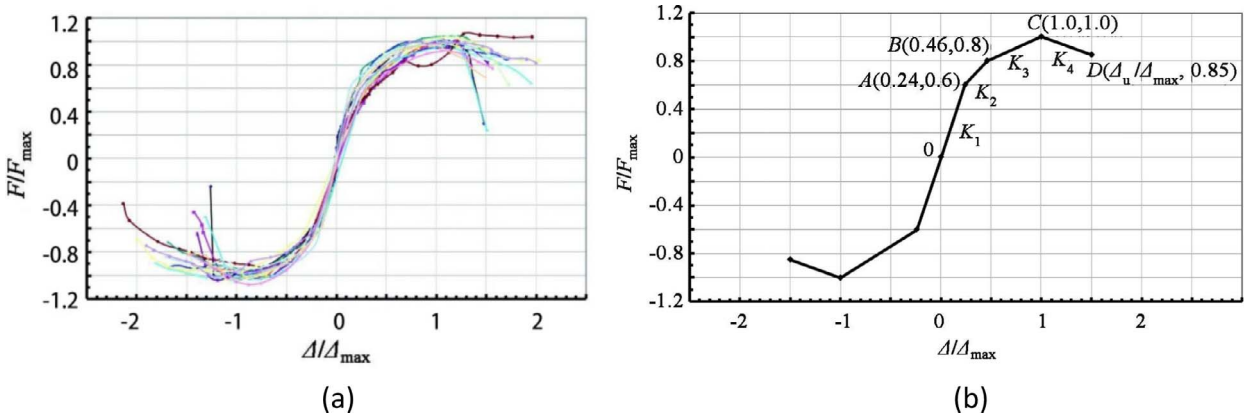

Fig. 11. Skeleton curves. (a) Dimensionless skeleton curves; (b) A simplified four-line skeleton curve.

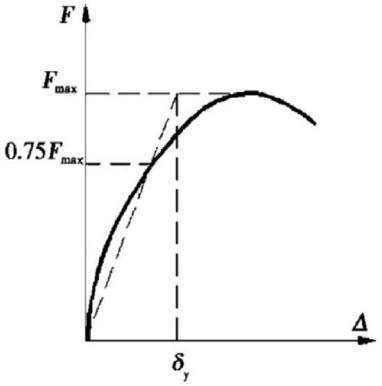

Fig. 12. Definition of yield point.

$$\left.\begin{aligned}&\begin{Bmatrix}ab\\de\end{Bmatrix}: \frac{F}{F_y}=\frac{4\Delta}{\Delta_y}\pm 3\\&\begin{Bmatrix}bc\\ef\end{Bmatrix}: \frac{F}{F_y}=\frac{\Delta}{\Delta_y}\pm 0.15\\&\begin{Bmatrix}cd\\fa\end{Bmatrix}: \frac{F}{F_y}=\frac{0.85\Delta}{\Delta_y}\pm 0.15\end{aligned}\right\} \tag{4}$$

The fitting result of tri linear and test data can be seen in Fig. 13(a): the coordinate of a is $(-1.0, -1.0)$; the coordinate of b is $(-0.95, -0.8)$; the coordinate of c is $(0, 0.15)$.

The standard hysteresis loop near peak point can be described by Eq. (5).

$$\left.\begin{aligned}&\begin{Bmatrix}a'b'\\d'e'\end{Bmatrix}: \frac{F}{F_{max}}=\frac{2.5\Delta}{\Delta_{max}}\pm 1.5\\&\begin{Bmatrix}b'c'\\e'f'\end{Bmatrix}: \frac{F}{F_{max}}=\frac{0.84375\Delta}{\Delta_{max}}\pm 0.175\\&\begin{Bmatrix}c'd'\\f'a'\end{Bmatrix}: \frac{F}{F_{max}}=\frac{0.825\Delta}{\Delta_{max}}\pm 0.175\end{aligned}\right\} \tag{5}$$

The fitting result of tri linear and test data can be seen in Fig. 13(b): the coordinate of a' is $(-1.0, -1.0)$; the coordinate of b' is $(-0.8, -0.5)$; the coordinate of c' is $(0, 0.175)$.

5.1.3. Stiffness degradation rule

Equivalent stiffness at yield point and peak point can be compared when the hysteresis loop in Fig. 13(a) and (b) are in the same coordinates system, as can be seen in Fig. 13(c). Obviously, each line of the hysteresis loop shows degradation from yield to peak load. The stiffness of yield hysteresis loop is K_y, and the stiffness of peak hysteresis loop is K_{max}. Degradation stiffness K_T can be described as:

$$K_T = K_{max} + (K_y - K_{max})\frac{1-\Delta/\Delta_{max}}{1-\Delta_y/\Delta_{max}} \tag{6}$$

Eq. (6) exhibits the rule of stiffness degradation from the aspect of test fitting. Stiffness K_y and K_{max} can be expressed in Eq. (7) corresponding to each line segment in Fig. 13(a) and (b).

$$\left.\begin{aligned}&K_y = F_y/\Delta_y \quad (K_{max} = 0.84375F_{max}/\Delta_{max})\\&K_y = 0.85F_y/\Delta_y \quad (K_{max} = 0.825F_{max}/\Delta_{max})\\&K_y = 4F_y/\Delta_y \quad (K_{max} = 2.5F_{max}/\Delta_{max})\end{aligned}\right\} \tag{7}$$

When skeleton curves, standard hysteresis loops and stiffness degradation rule are combined with each other, a complete hysteretic curve model can be obtained as shown in Fig. 14.

5.2. Shearing capacity formula generalization

The shearing capacity is very important in structural design. The shear capacity of SPRWs is calculated through superposition method, i.e. adding the capacity of concrete, steel section (channel) and steel plate. The first two items are calculated by equation in JGJ138—2016 Code for design of composite structures [33], i.e. V_c and V_s. The equation is shown as follows:

$$V_c = \frac{1}{\lambda - 0.5}\left(0.05f_c bh_0 + 0.13N\frac{A_w}{A}\right) + f_{yv}\frac{A_{sh}}{S}h_0 \tag{8}$$

$$V_s = \frac{0.4}{\lambda}f_a A_a \tag{9}$$

The capacity of the steel plate V_p is obtained by subtracting V_c and V_s from the measured tested capacity, and then an equation to represent the capacity of steel plate can be regressed from the test data, shown as follows:

$$V_p = \frac{0.22}{\lambda}f_P A_P \tag{10}$$

Therefore, the shearing capacity of SPRW is:

$$V = \frac{1}{\lambda - 0.5}\left(0.05f_c bh_0 + 0.13N\frac{A_w}{A}\right) + f_{yv}\frac{A_{sh}}{S}h_0 + \frac{0.4}{\lambda}f_a A_a + \frac{0.22}{\lambda}f_P A_P \tag{11}$$

In Eq. (11): λ is the aspect ratio of the wall, i.e. shear-to-span ratio of the calculated cross section; f_c is the compressive strength of concrete; b and h_0 are the thickness and effective depth of the web wall section, respectively; N is the compressive axial load applied to the wall; A_w and A are the cross-sectional area of the web wall and the gross cross-sectional area of the flanged wall, respectively (for rectangle section wall, $A_w = A$); f_{yv} and A_{sh} are the yield strength and cross-sectional areas of the horizontally distributed rebars; S is the spacing of the

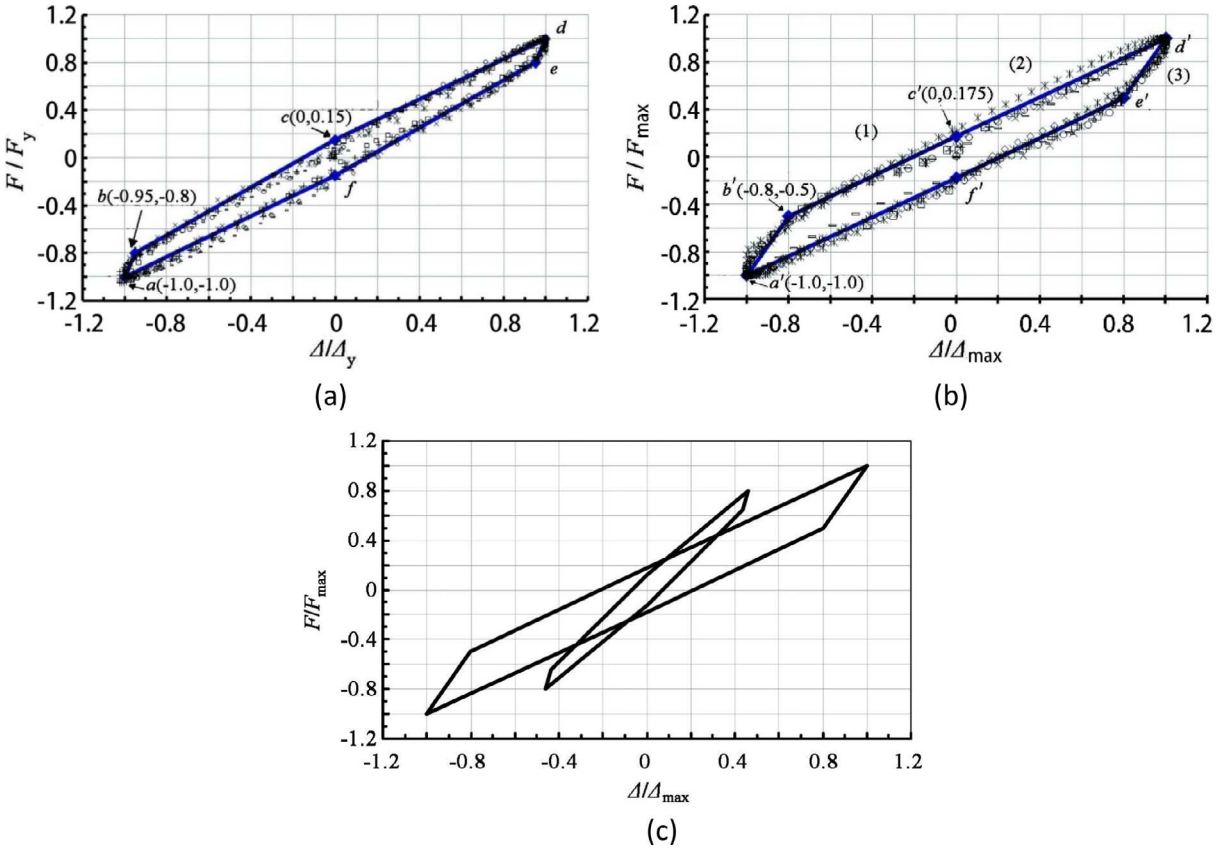

Fig. 13. Force-deformation generalization. (a) Point of F_y; (b) Point of F_{max}; (c) Point of F_y and F_{max} in the same coordinates system.

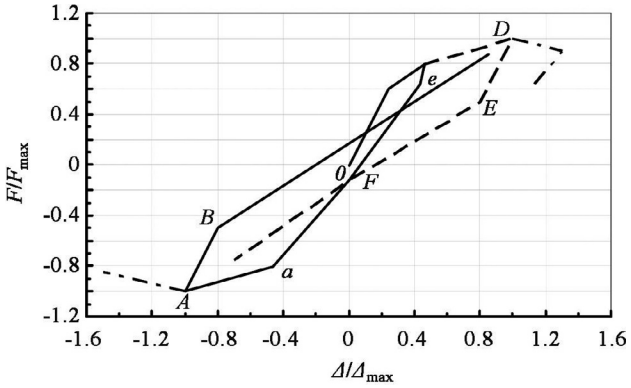

Fig. 14. Hysteretic curve model.

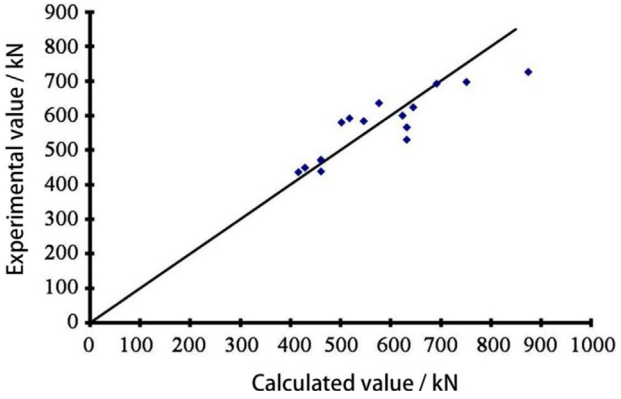

Fig. 15. Comparison of maximum shear capacity between experiment and calculation.

horizontal web bars; f_a and f_p are the yield strengths of the encased steel channel and steel plate, respectively; A_a and A_p are the cross-sectional areas of the encased steel channel and steel plate, respectively.

Comparing the experimental data with the calculated results, it can be seen that Eq. (11) can fit the shear bearing capacity of most steel plate reinforced concrete composite shear walls with an error within 10%, as shown in Fig. 15.

6. Conclusion

The seismic behavior of steel plate reinforced concrete composite shear wall is systematically investigated. A total of 16 SPRW specimens and 3 traditional RC walls with various parameters are designed, the corresponding low cyclic tests are implemented to study the seismic performance, including failure phenomena, failure mechanism, load carrying capacity, ductility and energy dissipation characteristics, etc. The key influence of some important parameters, e.g. aspect ratio, thickness of the wall and the steel plate, structural detailing, on the seismic behavior of SPRW is also analyzed based on the extensive experimental results. Finally, the hysteretic curve model and shearing capacity are generalized based on massive test data, and the design formula of shearing capacity is also proposed based on current design codes. The main conclusions are listed as follows:

(1) Compared to RC shear walls, the load capacity and ultimate displacement of SPRWs are increased by 106.99% and 121.96%. The ductility index and equivalent viscous damping coefficient are increased by 25.02% and 24.99% on average, respectively. SPRW has obvious better seismic performance than the traditional RC shear wall.
(2) Thickness of the wall and thickness of the steel plate are the main factor with regard to bearing capacity. Concrete plays an important

role in restraining the local buckling of the steel plate. A certain thickness of the steel plate can ensure ductility of the wall. The thickness of the wall is the most important parameter to increase deformability, ductility and energy dissipation capacity, followed by detailing and thickness of the steel plate. Compared with lateral ties, the structural detailing of shear studs on steel plates is more effective.

(3) When designing the SPRW, the maximum shear of the wall section can be evaluated by the proposed equation shown in Section 5.2 in this paper.

Acknowledgements

Financial support from the National Key Research and Development Program of China (2016YFC0701101) is highly appreciated. This work is also supported by National Natural Science Foundation of China (No. 51578449) and the Fundamental Research Funds for the Central Government Supported Universities.

Appendix A. Supplementary material

Supplementary data associated with this article can be found, in the online version, at http://dx.doi.org/10.1016/j.engstruct.2018.01.050.

References

[1] Lu Z, Chen XY, Zhang DC, Dai KS. Experimental and analytical study on the performance of particle tuned mass dampers under seismic excitation. Earthquake Eng Struct Dyn 2017;46(5):697–714.
[2] Lu Z, Wang DC, Masri SF, Lu XL. An experimental study of vibration control of wind-excited high-rise buildings using particle tuned mass dampers. Smart Struct Syst 2016;18(1):93–115.
[3] Lu Z, Lu XL, Jiang HJ, Masri SF. Discrete element method simulation and experimental validation of particle damper system. Eng Comput 2014;31(4):810–23.
[4] Lu Z, Huang B, Zhou Y. Theoretical study and experimental validation on the energy dissipation mechanism of particle dampers. Struct Control Health Monit 2017. http://dx.doi.org/10.1002/stc.2125.
[5] Lu Z, Chen XY, Zhou Y. An equivalent method for optimization of particle tuned mass damper based on experimental parametric study. J Sound Vib 2017. http://dx.doi.org/10.1016/j.jsv.2017.05.048.
[6] Lu Z, Wang ZX, Masri SF, Lu XL. Particle impact dampers past present and future. Struct Control Health Monit 2018;25(1):e2058. 1.
[7] Richard B, Martinelli P, Voldoire F, Corus M, Chaudat T, Abouri S, et al. SMART 2008: Shaking table tests on an asymmetrical reinforced concrete structure and seismic margins assessment. Eng Struct 2015;105:48–61.
[8] Panagiotou M, Restrepo JI, Conte JP. Shake-table test of a full-scale 7-story building slice. Phase I: Rectangular wall. J Struct Eng 2011;137(6):691–704.
[9] Emori K. Compressive and shear strength of concrete filled steel box wall. Steel Struct 2002;68(2):29–40.
[10] Zhou Y, Lu X, Dong Y. Seismic behaviour of composite shear walls with multi-embedded steel sections. Part I: Experiment. Struct Des Tall Special Build 2010;19(6):618–36.
[11] Dan D, Fabian A, Stoian V. Nonlinear behavior of composite shear walls with vertical steel encased profiles. Eng Struct 2011;33(10):2794–804.
[12] Wu YT, Kang DY, Yang YB. Seismic performance of steel and concrete composite shear walls with embedded steel truss for use in high-rise buildings. Eng Struct 2016;125:39–53.
[13] Ji X, Leong T, Qian J, Qi W, Yang W. Cyclic shear behavior of composite walls with encased steel braces. Eng Struct 2016;127:117–28.
[14] Zhao Q, Astaneh-Asl A. Cyclic behavior of traditional and innovative composite shear walls. J Struct Eng 2004;130(2):271–84.
[15] Astaneh-Asl A, Zhao Q. Cyclic behavior of steel shear wall systems [C]// Annual Stability Conference. Seattle: Structural Stability Research Council, Bethlehem, PA, US; 2002, p. 21–36.
[16] Rassouli B, Shafaei S, Ayazi A, Farahbod F. Experimental and numerical study on steel-concrete composite shear wall using light-weight concrete. J Constr Steel Res 2016;126:117–28.
[17] Li X, Li X. Steel plates and concrete filled composite shear walls related nuclear structural engineering: experimental study for out-of-plane cyclic loading. Nucl Eng Des 2017;2017(315):144–54.
[18] Qin Y, Shu GP, Fan SG, Lu J, Cao S, Han J. Strength of double skin steel-concrete composite walls. Int J Steel Struct 2017;17(2):535–41.
[19] Nguyen NH, Whittaker AS. Numerical modelling of steel-plate concrete composite shear walls. Eng Struct 2017;150:1–11.
[20] Guo L, Rong Q, Qu B, Liu J. Testing of steel plate shear walls with composite columns and infill plates connected to beams only. Eng Struct 2017;136:165–79.
[21] Wang B, Jiang H J, Lu X L. Seismic performance of steel plate-reinforced concrete composite shear wall [C]// Portugal: The 15th World Conference on Earthquake Engineering; 2012. p. 1–9.
[22] Saari WK, Hajjar JF, Schultz AE, Shield CK. Behavior of shear studs in steel frames with reinforced concrete infill walls. J Constr Steel Res 2004;60(10):1453–80.
[23] Dan D, Fabian A, Stoian V. Theoretical and experimental study on composite steel–concrete shear walls with vertical steel encased profiles. J Constr Steel Res 2011;67(5):800–13.
[24] Gan CJ, Lu XL, Wang W. Seismic behavior of steel plate reinforced concrete shear walls[C]//Beijing: 14th world conference on earthquake engineering; 2008. p. 89–96.
[25] Wang B, Jiang H, Lu X. Seismic performance of steel plate reinforced concrete shear wall and its application in China Mainland. J Constr Steel Res 2017;131:132–43.
[26] Wang B, Jiang H. Experimental study on seismic performance of steel plate reinforced concrete tubes under cyclic loading. Structural Design of Tall & Special Buildings; 2016.
[27] Wang B, Jiang H, Lu X. Experimental and numerical investigations on seismic behavior of steel truss reinforced concrete core walls. Eng Struct 2017;140:164–76.
[28] Mander JB, Priestley MJN, Park R. Theoretical stress-strain model for confined concrete. J Struct Eng, ASCE 1988;114(8):1804–26.
[29] Zhu BL. Structure seismic test. Beijing: Seismological Press; 1989. p. 141–2 [in Chinese].
[30] Park R. Ductility Evaluation from Laboratory and Analytical Testing [C]// Tokyo, Japan: Proceedings of 9th Word Conference on Earthquake Engineering - 9WCEE, vol. 8; 1988, p. 605–16.
[31] Park R. Valuation of ductility of structures and structural assemblages from laboratory testing. Bullet New Zealand Nat Soc Earthquake Eng 1989;22(3):155–66.
[32] Lu XL. Seismic theory of complex high-rise structures with application[C]//Beijing: Science Press; 2007 [in Chinese].
[33] JGJ138—2016 Code for design of composite structures [S]. Beijing: China Architecture & Building Press; 2016 [in Chinese].